Material distribution-based topology optimization for wave propagation problems

Ahmad H. Bokhari

Doctorate Thesis, April 2022
Department of Computing Science
Umeå University
Sweden

Department of Computing Science
Umeå University
SE-901 87 Umeå, Sweden
www.cs.umu.se

ISBN 978-91-7855-749-3 (Print)
ISBN 978-91-7855-750-9 (PDF)
ISSN 0348-0542
UMINF 22.05

Electronic version available at http://umu.diva-portal.org
Printed by: CityPrint i Norr AB, Umeå, Sweden 2022

Abstract

This thesis employs material distribution-based topology optimization for wave propagation problems. In the material distribution approach, we define a material indicator function that models the presence and absence of material in a design domain. By placing material inside the design domain, the aim is to design a device that maximizes the output power or transmission of the system. The time-harmonic linear wave propagation problem is modeled using the Helmholtz equation. The governing equation is solved using the finite element method, and an artificial boundary condition is used to truncate the domain. Moreover, a gradient-based algorithm, the method of moving asymptotes by Svanberg, is used to solve the optimization problem. An adjoint method efficiently computes the gradients of the objective function with respect to design variables.

This thesis considers two types of wave propagation problems: acoustic (Papers I–III) and electromagnetic wave propagation (Papers IV–V). In Papers I–II, we consider a bandpass design of a subwoofer. The aim of Paper I is to reduce the computational time required to evaluate the performance of a given subwoofer layout. To accomplish this, we develop a computationally efficient hybrid 2D–3D model. A full 3D model, as well as a lumped model, validate the hybrid model's results. Paper II focuses on optimizing the topology of a subwoofer using the computationally efficient hybrid model from Paper I for single as well multiple frequencies. In Paper III, we design a highly efficient uni-directional linear acoustic waveguide. Moreover, we also challenge the use of the term *acoustic diode* for such uni-directional linear acoustic waveguides in literature. Paper IV deals with the design of a microwave frequency dividing multiplexer, which splits the incoming signals into two frequency bands and delivers them to their respective output ports. In Paper V, we use the adjoint method to perform the sensitivity analysis of a coupled plasmonic problem where a Helmholtz equation is coupled to the Poisson equation. We validate the sensitivities computed using the adjoint method with the finite difference approach.

Sammanfattning på svenska

Denna avhandling använder materialdistributionsbaserad topologioptimering för vågutbredningsproblem. I materialdistributionsbaserad definierar vi en indikatorfunktion för material som modellerar närvaron och frånvaron av material i en designdomän. Genom att placera material inom designdomänen är syftet att designa en enhet som maximerar utgångseffekten eller överföringen av systemet. Det tidsharmoniska linjära vågutbredningsproblemet modelleras med hjälp av Helmholtz-ekvationen. Den styrande ekvationen löses med finita elementmetoden, och ett artificiellt gränsvillkor används för att trunkera domänen. Dessutom används en gradientbaserad algoritm, metoden för rörliga asymptoter av Svanberg, för att lösa optimeringsproblemet. En adjoint metod beräknar effektivt gradienterna för målfunktionen med avseende på designvariabler.

Denna avhandling behandlar två typer av vågutbredningsproblem: akustiska (Artikel I-III) och elektromagnetisk vågutbredning (Artikel IV-V). I Artikel I-II betraktar vi en bandpassdesign för en subwoofer. Syftet med Artikel I är att minska beräkningstiden som krävs för att utvärdera prestandan hos en given subwooferlayout. För att åstadkomma detta utvecklar vi en beräkningseffektiv hybrid 2D–3D-modell. En fullständig 3D-modell, såväl som en sammanlagen modell, validerar hybridmodellens resultat. Artikel II fokuserar på att optimera topologin hos en subwoofer med hjälp av den beräkningseffektiva hybridmodellen från Artikel I för såväl enstaka som flera frekvenser. I Artikel III designar vi en mycket effektiv enkelriktad linjär akustisk vågledare. Dessutom utmanar vi också användningen av termen akustisk diod för sådana enkelriktade linjära akustiska vågledare i litteraturen. Artikel IV handlar om konstruktionen av en mikrovågsfrekvensdelande multiplexer, som delar upp de inkommande signalerna i två frekvensband och levererar dem till deras respektive utgångsportar. I Artikel V använder vi adjoint-metoden för att utföra känslighetsanalysen av ett kopplat plasmoniskt problem där en Helmholtz-ekvation är kopplad till Poisson-ekvationen. Vi validerar känsligheterna som beräknas med hjälp av adjoint-metoden med finita differensmetoden.

List of papers

The thesis is based on the following papers:

Paper I A.H. Bokhari, M. Berggren, D. Noreland, and E. Wadbro. A computationally efficient hybrid 2D–3D subwoofer model. *Scientific Report* ***11****, 255* (2021).

Paper II A.H. Bokhari, M. Berggren, D. Noreland, and E. Wadbro. Topology optimization of a subwoofer. *Submitted manuscript* (2022).

Paper III A.H. Bokhari, A. Mousavi, B. Niu, and E. Wadbro. Topology optimization of an acoustic diode? *Structural and Multidisciplinary Optimization* ***63****, 2739–2749* (2021).

Paper IV A.H. Bokhari, E. Hassan, and E. Wadbro. Topology optimization of a microwave frequency dividing multiplexer. *Submitted manuscript* (2022).

Paper V A.H. Bokhari and E. Wadbro. Sensitivity analysis of a coupled plasmonic problem. *Technical report* UMINF 22.04 (2022).

Acknowledgments

First and foremost, I would like to thank my supervisor, Eddie Wadbro. His advise and support helped me through all stages of my PhD. Even during his busy schedule, he was always available for guidance. Second, I would like to thank Martin Berggren for his advice and direction during my Ph.D.

I thank all my colleagues in *Computing Science Department*, *UMIT Reseach Lab*, and *Design Optimization Group* for providing a pleasant working environment. Special thanks to Emadeldeen Hasan, Juan Carlos Araujo-Cabarcas, and Abbas Mousavi for all the discussions, support, and advice.

I am extremely grateful to my parents for all their love, care, and support. Finally, I would express my gratitude to my wife for her unwavering support and understanding.

Contents

Chapter 1

Introduction

Our goal when designing a component or a system is to get the best performance out of it. The decision-making process of selecting the best design that meets the requirements is called optimization. In simple words, optimization is doing the best with available resources. In engineering, design optimization is a methodology that uses a mathematical formulation to solve this task. The purpose of this methodology is to obtain an optimal design relative to a defined criteria. The optimal design is obtained by extremizing an objective function subject to constraints. The objective function can be a measure of, for example, efficiency, power, compliance, fatigue, stress, or cost.

Design optimization is commonly used for structural mechanics problems, and it can be classified into three categories: sizing, shape, and topology optimization. In sizing optimization, the design variable is, for example, the thickness or cross-section of the structure (truss or beam). An optimal thickness minimizes compliance (or deflection) of the structure subject to constraints. In shape optimization, the boundary of the structure can be varied to minimize or maximize an objective function. Finally, topology optimization is the most general technique. In topology optimization, we vary the layout of the material in a given domain to minimize or maximize an objective function subject to constraints. Unlike sizing and shape optimization, topology optimization allows the design to assume any configuration in the given domain to maximize or minimize an objective function without being constrained by predefined configurations.

Topology optimization allows better material utilization by decreasing the structure's weight, and hence, its cost. Moreover, it aids the designers to discover novel designs. This method has been successfully used to design structures, such as bridges [37], modern vehicle chassis [12], and airplane wings [3] and fuselages [68]. Over the last two decades, researchers have made efforts to extend this method to other fields such as fluid flow, heat transfer, and wave propagation problems. In this thesis, we deal with the design of wave propagation problems using topology optimization.

Chapter 2

Topology Optimization

Topology optimization is a technique for determining the optimal material layout in a given domain. The topology optimization method was first introduced to minimize the compliance of a linear elastic structure. Compliance is a measure of structure's deflection (or deformability) subject to static loading. In 1977, Prager and Rozvany [44] presented the optimal layout theory for grillages based on an earlier work on trusses [38]. A decade later, Bendsoe and Kikuchi [9] applied the homogenization method for structural design optimization, and proposed an interpolation scheme based on a power-law to improve convergence to a black and white design. Researchers [39, 65] later termed this interpolation scheme the SIMP (*solid isotropic material with penalization*) method. SIMP is now widely used to solve compliance problems [7, 20, 46, 48]. The existing strategies for topology optimization of structures are summarized in a review by Rozvany [45]. In addition, the monograph by Bendsoe and Sigmund [10] discusses in detail the topology optimization of structural problems, as well as its extension in other fields, such as fluid flow, wave propagation, and non-linear problems.

For compliance minimization problems, topology optimization techniques are well established, and reliable tools are available to handle them. Educational articles that solve 2D compliance problems like 88-line [6] and 99-line [47] MATLAB codes are good for educational and research purposes. In addition, the Python code [69] by Zuo and Xie allows solving 3D topology optimization problems with complex geometries, as it can read data from CAD files. Another 3D code [36] can be used to solve compliance and heat conduction problems. Today, topology optimization tools for structural mechanics problems are also available in CAE (computer-aided engineering) software such as COMSOL [29], Solidworks [49], and ALTAIR [56]. However, the range of problems they can handle is still limited.

Topology optimization has become an important tool for engineering design in the automotive [12, 64] and aerospace [3, 68] industries. The methods for structural design optimization have matured over the last three decades.

Therefore, researchers have attempted to extend topology optimization techniques to other fields, such as fluid flow [4, 11, 17], heat transfer [15, 16, 66], and wave propagation problems. Early research on topology optimization for wave propagation problems was carried out in 1999 by Dobson and Cox [18]. The aim was to maximize the band gaps in photonic crystals and the Helmholtz equation was used to model time-harmonic wave propagation. The method was later applied to the design of acoustic problems such as improving transmission efficiency of an acoustic horn [58] and an acoustic lens [60], noise reduction in room [19], and a sound muffler [33]. Moreover, the topology optimization technique has gained popularity in the last decade for the design of electromagnetic problems such as waveguide filters [1], electric and magnetic resonators [2], and metallic antennas [25, 61].

2.1 The Material Distribution Method

The so-called material distribution approach is most commonly used for topology optimization. This approach models the presence of material by a material indicator function α, where $\alpha(x) = 1$ and $\alpha(x) = 0$ represent two materials (solid and air). For the computer implementation of this approach, we use a raster representation for a 2D setup and a voxel representation for a 3D setup. More precisely, a fixed domain (also referred to as the design domain) is divided into elements. The optimization problem consists of finding the element values $\alpha_i \in \{0, 1\}$ to extremize a given performance measure (objective function) subject to constraints.

Numerical methods, such as the finite difference [31], finite element [32], or finite volume [40] method are used for the discretization of the governing PDE. The finite element method is widely used as a PDE solver for topology optimization problems. However, the finite volume and finite difference methods are often preferred for fluid flow problems [17, 21] and the time-domain problems such as Maxwell's equations [25, 41], respectively. For the wave propagation problems in this thesis, the finite element method is used.

By discretizing the governing equation using the finite element method, we assemble a state equation of the form

$$\boldsymbol{A}(\boldsymbol{\alpha})\boldsymbol{u} = \boldsymbol{b}, \tag{2.1}$$

where the matrix $\boldsymbol{A}$ depends on the governing equation (such as the Poisson or Helmholtz equation) and boundary conditions (such as Dirichlet, Neumann, or absorbing boundary condition), $\boldsymbol{u}$ is a state vector (such as displacement or pressure), vector $\boldsymbol{\alpha}$ specifies the design variables, and vector $\boldsymbol{b}$ is the forcing of the system.

Using the definitions above, the optimization problem is written as

$$\begin{aligned} &\min_{\boldsymbol{\alpha}} J(\boldsymbol{\alpha}) \\ &\text{such that } \boldsymbol{A}(\boldsymbol{\alpha})\boldsymbol{u} = \boldsymbol{b} \\ &\qquad \alpha_i \in \{0,1\}, \quad i = 1,2,\ldots,N, \end{aligned} \tag{2.2}$$

where J is the objective function, α_i is the element value of design variable, and N is the number of elements in the design domain.

2.2 Relaxation

The approach presented above ending in expression (2.2) uses a discrete parameterization of the design problem, in which α_i can either be a 0 or 1. This class of problems is computationally expensive, particularly when dealing with large-scale optimization problems involving millions of design variables. To make this problem tractable, we allow the material indicator function to be continuous, that is, $\alpha_i \in [0,1]$. This relaxation enables us to use gradient-based optimization algorithms like the optimality criteria (OC) [8, 47] and the method of moving asymptotes (MMA) [53]. These algorithms require gradients of the objective function with respect to design variables, which are efficiently computed using the adjoint variable method [22]. The optimization problem for the relaxed material indicator function can be written as

$$\begin{aligned} &\min_{\boldsymbol{\alpha}} J(\boldsymbol{\alpha}) \\ &\text{such that } \boldsymbol{A}(\boldsymbol{\alpha})\boldsymbol{u} = \boldsymbol{b} \\ &\qquad 0 \leq \alpha_i \leq 1, \quad i = 1,2,\ldots,N. \end{aligned} \tag{2.3}$$

However, the intermediate values of material indicator function are not desirable. We want elements to either hold material or void. Thus, we employ a combination of filtering and penalization methods to suppress intermediate values of material indicator function and impose size control on geometrical features of design.

For compliance minimization problems, the most common method for penalizing the intermediate values of design variables is the SIMP method. A volume constraint is added to obtain an optimal design; otherwise, SIMP penalizes all the elements toward solid material. The SIMP interpolation scheme for the filtered design vector $\mathcal{F}(\boldsymbol{\alpha})$ is defined as

$$\boldsymbol{A}\big(\mathcal{F}(\boldsymbol{\alpha})^p\big) = \sum_{i=1}^{N} \Big(\alpha_{\min} + (1-\alpha_{\min})\mathcal{F}(\boldsymbol{\alpha})_i^p\Big)\boldsymbol{A}_i, \tag{2.4}$$

where $p > 1$ is a penalty parameter, $\alpha_{\min} > 0$, and $\boldsymbol{A}_i$ is the element stiffness matrix for the compliance minimization problem. A zero lower bound on design variables ($\alpha_{\min} = 0$) makes the rows in state matrix $\boldsymbol{A}$ vanish, resulting in a

singular matrix. To obtain a unique solution, the SIMP interpolation scheme avoids this issue by choosing $\alpha_{\min}$ as a small positive constant, for example $\alpha_{\min} = 10^{-3}$.

The optimization problem with filtering, SIMP penalization, and a volume constraint V is

$$\begin{aligned} &\min_{\boldsymbol{\alpha}} J\big(\mathcal{F}(\boldsymbol{\alpha})^p\big) \\ &\text{such that } \boldsymbol{A}\big(\mathcal{F}(\boldsymbol{\alpha})^p\big)\,\boldsymbol{u} = \boldsymbol{b} \\ &\qquad \frac{1}{N}\sum_{i=1}^{N} \alpha_i \leq V \\ &\qquad 0 \leq \alpha_i \leq 1, \quad i = 1, 2, \ldots, N. \end{aligned} \tag{2.5}$$

If we use a value of p large enough the intermediate values of $\boldsymbol{\alpha}$ are suppressed.

2.3 Topology Optimization for Wave Propagation Problems

For acoustic wave propagation problems, we employ a material distribution approach that is analogous to the standard approach used for the compliance problem. More precisely, the material indicator function acts directly on the domain integrals, where $\alpha(x) = 1$ represents air and $\alpha(x) = \varepsilon$ represents solid. Using $\alpha = 0$ as the lower bound of the design variables again causes the state matrix $\boldsymbol{A}$ in expression (2.1) to be singular. To solve this problem, we use $\alpha \in [\varepsilon, 1]$. For the acoustic problems in this thesis, we use $\varepsilon = 10^{-3}$. This method can at least be traced back to the study of an acoustic horn [58] by Wadbro and Berggren. Moreover, for this approach, there exists a proof [30] that the problem with ε as the lower bound of the design variable converges linearly in ε to the problem with the exactly modeled scatterer in the air domain.

As stated earlier, we employ a combination of penalization and a nonlinear filtering method to suppress intermediate values of design variables and impose size control on the design. For the penalization of design variables, we do not use SIMP for the wave propagation problems. Instead, for the acoustic wave propagation, we add an explicit term to the objective function for penalization, as proposed by Allaire and Kohn [5]. Furthermore, we do not impose a volume constraint, allowing the optimizer to place as much material as it wants to achieve the best design.

For the filtering of design variables, we use the fW-mean filtering framework by Wadbro and Hägg [59]. We approximate morphological operators like erode and dilate, using the non-linear harmonic mean filters [54]. The harmonic erode and dilate operators, which act on the design vector $\boldsymbol{\alpha}$, are defined in the discrete setting as follows:

$$\mathcal{E}_{r,\beta}(\boldsymbol{\alpha}) = \boldsymbol{f}_{\mathcal{E}_\beta}^{-1}\big(\boldsymbol{W}_r \boldsymbol{f}_{\mathcal{E}_\beta}(\boldsymbol{\alpha})\big) \quad \text{and} \quad \mathcal{D}_{r,\beta}(\boldsymbol{\alpha}) = \boldsymbol{f}_{\mathcal{D}_\beta}^{-1}\big(\boldsymbol{W}_r \boldsymbol{f}_{\mathcal{D}_\beta}(\boldsymbol{\alpha})\big), \tag{2.6}$$

where the weight matrix $\boldsymbol{W}_r$ implicitly defines the neighborhood $\mathcal{N}_i$ of element i. The filter radius r determines the neighbourhood size where for element i,

$$\mathcal{N}_i = \{j : \|x_i - x_j\| < r\}, \quad j \in \{1, 2, \ldots, N\}, \tag{2.7}$$

where x_i and x_j are the centroids of element i and j, respectively. More precisely, $\boldsymbol{W}_r = \boldsymbol{D}^{-1}\boldsymbol{G}_r$, where the diagonal matrix $\boldsymbol{D} = \operatorname{diag}\big(|\mathcal{N}_1|, |\mathcal{N}_2|, \ldots, |\mathcal{N}_N|\big)^T$ and the neighborhood matrix $\boldsymbol{G}_r$ with entries, $g_{ij} = 1$ if $j \in \mathcal{N}_i$, else $g_{ij} = 0$.

Moreover, $\boldsymbol{f}_{\mathcal{E}_\beta} = \big[f_{\mathcal{E}_\beta}(\alpha_1),\ f_{\mathcal{E}_\beta}(\alpha_2), \ldots, f_{\mathcal{E}_\beta}(\alpha_N)\big]^T$ and $\boldsymbol{f}_{\mathcal{D}_\beta} = \big[f_{\mathcal{D}_\beta}(\alpha_1),\ f_{\mathcal{D}_\beta}(\alpha_2), \ldots, f_{\mathcal{D}_\beta}(\alpha_N)\big]^T$ with entries $f_{\mathcal{E}_\beta}(\alpha_i) = (\alpha_i + \beta)^{-1}$ and $f_{\mathcal{D}_\beta}(\alpha_i) = f_{\mathcal{E}_\beta}(1 - \alpha_i)$, $i = 1, 2, \ldots, N$, respectively. Similarly, entries of $\boldsymbol{f}_{\mathcal{E}_\beta}^{-1}$ and $\boldsymbol{f}_{\mathcal{D}_\beta}^{-1}$ are $f_{\mathcal{E}_\beta}^{-1}(\alpha_i)$ and $f_{\mathcal{D}_\beta}^{-1}(\alpha_i)$, respectively, which are the inverse of $f_{\mathcal{E}_\beta}(\alpha_i)$ and $f_{\mathcal{D}_\beta}(\alpha_i)$. Here, $\beta > 0$ is a parameter that controls the properties of nonlinear filtering. Thus, we refer to it as nonlinearity parameter.

We define harmonic close by using harmonic erode and dilate in a series

$$\mathcal{C}_{r,\beta}(\boldsymbol{\alpha}) = \mathcal{E}_{r,\beta}\big(\mathcal{D}_{r,\beta}(\boldsymbol{\alpha})\big), \tag{2.8}$$

and finally, we define the filtering vector

$$\mathcal{F}(\boldsymbol{\alpha}) = \varepsilon + (1 - \varepsilon)\, \mathcal{C}_{r,\beta}(\boldsymbol{\alpha}), \tag{2.9}$$

which holds element values of filtered design variables.

The optimization problem with a quadratic penalization term, filtering of design variables, and ε as a lower bound is stated as

$$\begin{aligned} &\min_{\boldsymbol{\alpha} \in \mathcal{A}}\ J\big(\mathcal{F}(\boldsymbol{\alpha})\big) + \frac{\gamma}{N}(\boldsymbol{\alpha}^T - \varepsilon)(\mathbf{1} - \boldsymbol{\alpha}) \\ &\text{such that } \boldsymbol{A}\big(\mathcal{F}(\boldsymbol{\alpha})\big)\boldsymbol{x} = \boldsymbol{b}, \end{aligned} \tag{2.10}$$

where γ denotes the penalty parameter and the set of admissible designs is

$$\mathcal{A} = \big\{\boldsymbol{\alpha} \in \mathbb{R}^N \mid \varepsilon \leq \alpha_i \leq 1\big\}. \tag{2.11}$$

We employ MMA, a gradient-based algorithm, to solve optimization problems in this thesis. To avoid being early caught in a bad local minimum, we use a continuation approach for γ and β. To this end, we start the optimization with a small penalization value and linear filtering of design variables by controlling both the parameters. This is to ensure that the penalization of design variables and nonlinear filters for size control does not affect the optimization in the initial stage. More precisely, we start the optimization with a small value of the penalty parameter since penalization is almost negligible when the limit $\gamma \to 0$. Similarly, we start the optimization with a large value of the nonlinearity parameter because the filtering is essentially linear when the limit $\beta \to +\infty$. The optimization terminates, when the convergence criteria of MMA algorithm is met. In the next step, we provide the optimizer with the optimized design

from the previous step as an initial guess. Moreover, the penalty parameter is increased while the nonlinearity parameter is decreased. The quadratic term in objective function (2.10) becomes large as the limit $\gamma \to +\infty$, penalizing the design variables towards ε and 1. Moreover, the filtering behavior becomes nonlinear as the limit $\beta \to 0$, and the morphological operators impose size control on the design. We stop the optimization when we achieve a black and white design with size control and the optimizer's convergence criteria is met.

2.4 Alternate Methods for Topology Optimization

Another important approach for topology optimization is the level set method. This method has been successfully used for structural optimization [62]. The level set method determines the geometry of structure by defining an interface of material and void. It is also suitable for optimization of structural problems with geometric uncertainties [13, 24]. Level set methods have the disadvantage of being sensitive to the initial guess, which limits the final design. Furthermore, gradients of level set functions near the boundary have a significant impact on the convergence.

Earlier work [5, 9, 52] on topology optimization of structures was based around the homogenization method. For this approach, the topology optimization problem is defined as finding the ideal porosity of a porous medium by using an optimality criteria. A material model with micro-scale voids is employed. This approach can create designs with extremely fine microstructures that are sometimes impossible to manufacture. Different ways have been used to overcome this problem, the most common of which being SIMP, which penalizes intermediate values of design variables. For details on the homogenization method, see the review [26] and book [27] by Hassani and Hinton.

The topology optimization problem is defined using discrete values of design variables in expression (2.2). Therefore, it appears natural to solve the problem using a discrete optimization approach. Few problems have been solved using this approach [51, 55] because it is computationally expensive, and convergence is difficult to achieve. However, a recent study [43] by Picelli et al. presents an efficient method to use discrete design variables for topology optimization by solving compliance problems for multiple load cases.

Chapter 3

Summary of Papers

Wave propagation is an intriguing physical phenomenon. A wave can be regarded as an energy-carrying disturbance in a medium or a vacuum. Sound, light, water ripples, and earthquakes are some of the most familiar examples of waves we encounter in our daily lives. Moreover, modern electronic devices like mobile phones, televisions, and sound systems include loudspeakers, microphones, and antennas (e.g., Bluetooth, WiFi, cellular), which use acoustic and electromagnetic wave propagation. Hence, designing efficient devices is of interest to engineers and physicists, which motivates efforts to make topology optimization for wave propagation problems as successful as it is for structural mechanics problems. This thesis employs a material distribution approach for the topology optimization of wave propagation problems. The layout of this thesis is such that Papers I–III deal with topology optimization of acoustic wave propagation problems, while Papers IV–V deal with electromagnetic wave propagation problems.

3.1 Subwoofer, Papers I–II

3.1.1 Introduction

Separate transducers (or drivers) are utilized to generate low, mid, and high frequencies in a loudspeaker system. All signals are received via a crossover system, which divides them across different transducers based on their frequency range. A subwoofer is a type of loudspeaker that reproduces low frequencies in a loudspeaker system. Here, we present a bandpass design of a subwoofer. The bandpass design, as the name implies, enables a specific frequency range to pass while rejecting all frequencies outside of that range. In a bandpass subwoofer design, the transducer is housed in a sealed chamber and it radiates in a ported front chamber.

In Paper I, the aim is to reduce the computational time it takes to evaluate the performance of a given subwoofer layout. To this end, we develop a compu-

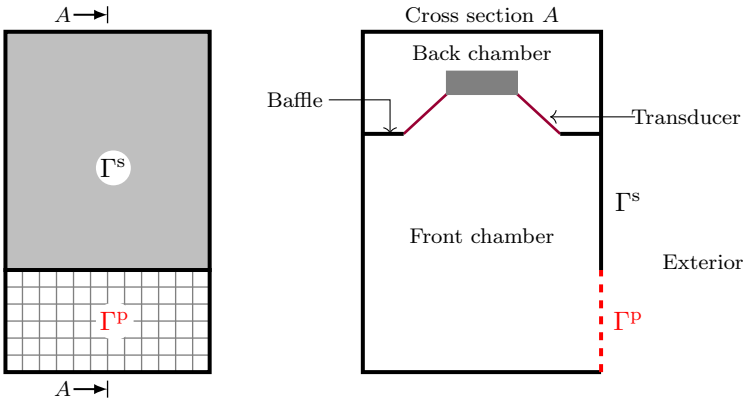

Figure 3.1: 3D model. Left: Front view of the subwoofer where the output port is divided into rectangular panels for impedance boundary condition. Right: Cross-section view of the subwoofer.

tationally efficient hybrid 2D–3D model. The results of the hybrid model are validated by a full 3D model as well as a lumped model. Paper II deals with the topology optimization of a subwoofer using the computationally efficient 2D–3D hybrid model.

3.1.2 Mathematical Modeling

Wave propagation inside the subwoofer cabinet and in the exterior is governed by the Helmholtz equation

$$\Delta p + k^2 p = 0, \tag{3.1}$$

where the wave number is $k = \omega/c$, in which ω is the angular frequency and c is the speed of sound, and p is the complex pressure amplitude.

The finite element method is used to discretize the Helmholtz equation inside the subwoofer cabinet, while the interaction of the subwoofer with the exterior through an output port is modeled using the boundary element method solving exterior Helmholtz problems. The walls of the subwoofer cabinet are assumed to be soundhard, which implies that

$$\frac{\partial p}{\partial n} = 0. \tag{3.2}$$

The amplifier receives an input voltage to actuate the transducer's electromagnetic coil, which moves the cone to generate sound. A lumped element model is used for modeling electromagnetic and mechanical parts of the transducer.

3D model

Consider the subwoofer setup illustrated in Fig. 3.1, where Γ^{p} and Γ^{s} denote the output port and the soundhard walls, respectively. In the 3D model, the

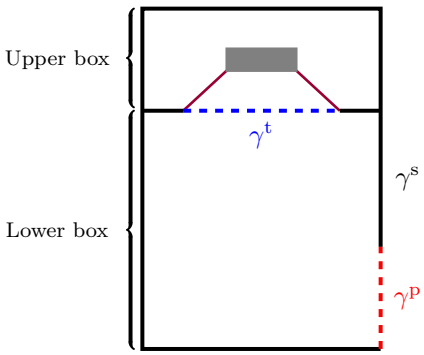

Figure 3.2: Hybrid model: Cross-section view of subwoofer.

subwoofer cabinet is divided into a front and a back chamber by the transducer and the baffle. We employ a full 3D model for the front and the back chamber, as well as the subwoofer exterior. Moreover, we use an impedance boundary condition to model the interaction of the subwoofer cabinet with the exterior. We use the concept of acoustic impedance to implement this boundary condition. The acoustic impedance provides a complete wave response to any external stimuli. In addition, it can be evaluated at a physical boundary between two mediums or a fictitious boundary such as the output port. It is defined as the ratio of complex pressure amplitude p to the velocity u,

$$Z = \frac{p}{u}, \tag{3.3}$$

where both p and u are dependent upon the frequency.

To implement an impedance boundary condition [42, 57], we truncate our domain at Γ^{p}. The boundary Γ^{p} is divided into N^{p} rectangular panels, as illustrated in Fig. 3.1 (left). To model the interaction of the subwoofer cabinet with the exterior, we assemble an $N^{\mathrm{p}} \times N^{\mathrm{p}}$ matrix $\boldsymbol{Z}^{\mathrm{p}}_{\mathrm{3D}}$ using an impedance relation that relates pressure and velocity at these panels. Impedance matrix $\boldsymbol{Z}^{\mathrm{p}}_{\mathrm{3D}}$ is assembled column-wise by setting a unit velocity at each panel and solving an exterior Helmholtz problem for each panel using the boundary element method. Impedance boundary condition allows the exterior problem to be solved independently of the interior problem. Thus, this allows us to divide our acoustic problem into two sub-problems, which can be solved independently. We pay a one-time cost by computing the impedance matrix for the output port, and then we evaluate the performance of various subwoofer layouts by simply solving the interior problem. A detailed description on the implementation of the impedance boundary condition is presented in Paper I.

Hybrid 2D–3D model

Consider the subwoofer setup, illustrated in Fig. 3.2, where γ^{p} and γ^{s} denote the output port and the soundhard walls, respectively, and γ^{t} divides the upper and the lower box. The lower box is modeled in 2D while the upper box and the exterior are modeled in 3D. We assume planar symmetry in the lower box due to long wavelengths and hence, use a 2D model. However, due to the transducer, 3D effects in the upper box are unavoidable.

For the computational efficiency, we divide our acoustic problem into three sub-problems by using the impedance boundary condition. The three sub-problems are: the lower box, the upper box including the transducer, and the exterior. We assemble a $(N^{\mathrm{t}}+1)\times(N^{\mathrm{t}}+1)$ matrix $\boldsymbol{Z}^{\mathrm{t}}$ to model the response of the upper box. We divide γ^{t} into depth-wise panels and the impedance matrix $\boldsymbol{Z}^{\mathrm{t}}$ is assembled columnwise by setting a unit velocity at these panels. In addition to these panels, the effect of the transducer's cone is also taken into consideration by setting a unit velocity at the cone. While a unit velocity is set at each panel and cone in succession, we compute the voice coil current and average pressure at each panel. Similarly, the response of the exterior has already been computed by assembling an impedance matrix for the 3D model.

The use of impedance boundary conditions allows us to pre-compute the response of the exterior and the upper box. Another advantage is that we can use different methods to solve different sub-problems. We use the finite element method to compute the response of the upper box, while we use the boundary element method to compute the response of the exterior. This modular approach makes the hybrid model computationally efficient. There is a one-time computational cost to pre-compute impedance matrices for the exterior and the upper box. Once, these matrices are computed, we efficiently evaluate the performance of different subwoofer layouts. Moreover, the hybrid model is also computationally feasible to be used in an optimization loop.

3.1.3 Optimization Problem

The hybrid model is used to optimize the subwoofer's cabinet, with the lower box serving as the design domain. By placing material inside the design domain, the objective is to maximize the subwoofer's output power for the target frequencies. We evaluate the subwoofer's radiated power $\mathcal{P}$ through the output port by integrating the acoustic intensity,

$$\mathcal{P} = \int_{\gamma^{\mathrm{p}}} p\, u^{\mathrm{p}}, \tag{3.4}$$

where p denotes the complex pressure amplitude inside the lower box and u^{p} denotes the normal velocity at the output port. In Paper II, the subwoofer's radiated output power is maximized for both single as well as multiple frequencies. The objective function that optimizes for the set of frequencies $f_1, f_2, \ldots, f_m$

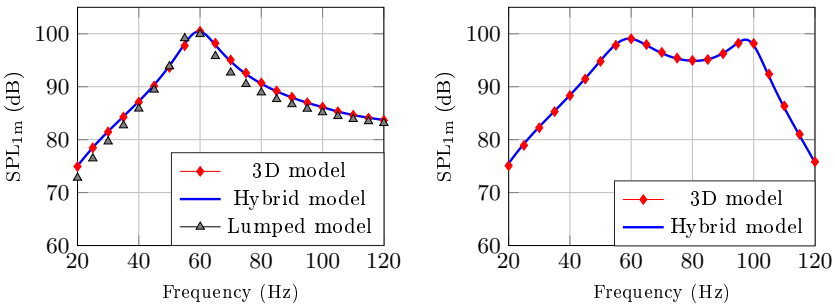

Figure 3.3: The SPL, 1m in front of the output port, is computed as the function of frequency. Left: Frequency response of the subwoofer with empty lower box. Right: Frequency response of subwoofer with a horizontal wall in the lower box.

is written as

$$J(\mathcal{F}(\boldsymbol{\alpha})) = \sum_{i=1}^{m} \ln\left(\mathcal{P}_{f_i}\right) \tag{3.5}$$

where $\mathcal{F}(\boldsymbol{\alpha})$ denotes the filtered design vector and m denotes the number of frequencies. Moreover, the sound pressure level (SPL) is measured 1 m in front of the output port to evaluate the performance of the subwoofer. It is a logarithmic scale measured in dB. To compute SPL for all the designs, 1 V is applied as the input voltage to the amplifier.

3.1.4 Selected results

In Paper I, we consider two layouts in the subwoofer's lower box to validate the hybrid model, an empty lower box as well as a horizontal wall inside the subwoofer's lower box. Fig. 3.3 (left) illustrates that the results of the hybrid and 3D model closely match each other for the first layout. Moreover, the results of a lumped model also follow the same trend. Fig. 3.3 (right) illustrates that the results of the hybrid and 3D model again closely match each other for the second layout. For the second subwoofer layout, we do not use a lumped model because they require modifications for each new subwoofer layout. Hence, they are not suitable for evaluating the performance of complex material layouts in the subwoofer's lower box.

In addition, we perform 20 simulations to compare the computational times of the 3D and hybrid models. For each simulation, we consider 21 frequencies in the range $20 - 120$ Hz for the time analysis. The mean times for the 3D model and the hybrid models for a given subwoofer layout are 19 minutes 12 seconds and 44.1 seconds, respectively. The difference in computational times is significant, which indicates that the 3D model is not suitable for use in an optimization loop. Therefore in Paper II, we employ the hybrid model for optimizing the material layout in the subwoofer's lower box.

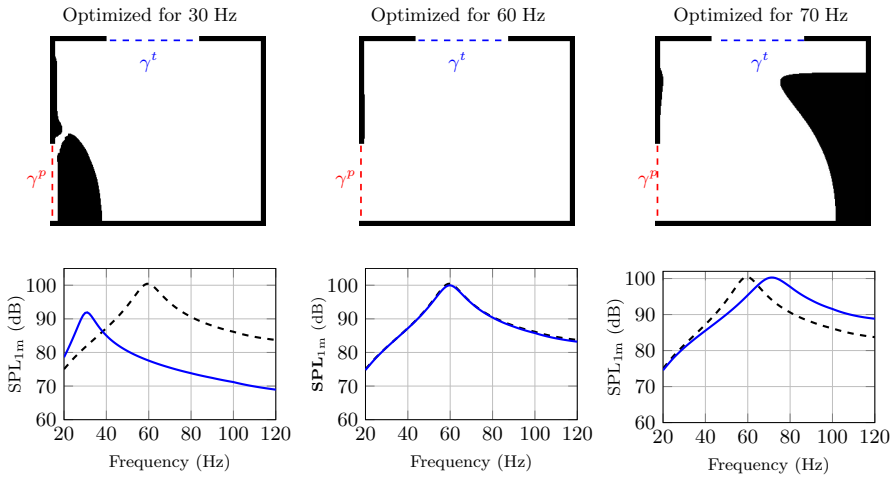

Figure 3.4: Single Frequency Optimization. Top: Optimized designs. Bottom: The SPL, 1m in front of the output port, is computed as the function of frequency.

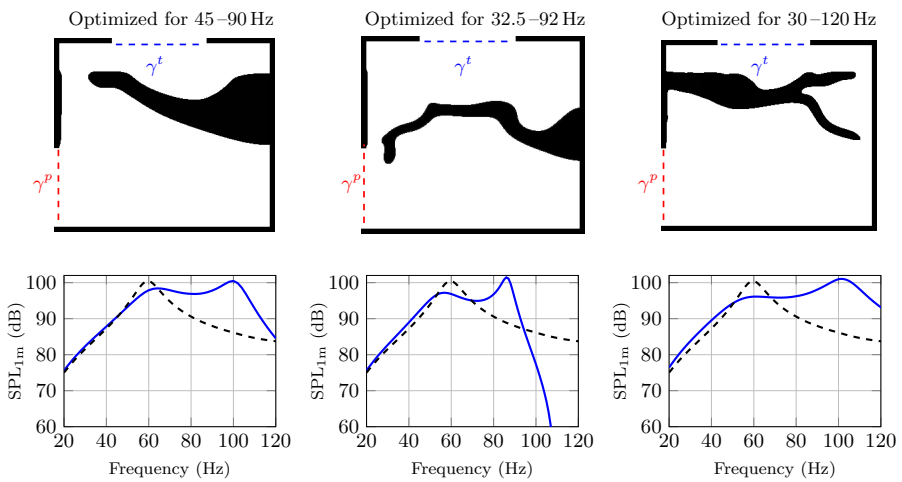

Figure 3.5: Multi Frequency Optimization: Top: Optimized designs. Bottom: The SPL, 1m in front of the output port, is computed as the function of frequency.

In Paper II, we compare the frequency response of the optimized designs with the frequency response of an empty lower box, which serves as a reference. The optimized designs along with the frequency responses for single target frequencies 30 Hz, 60 Hz, and 70 Hz are shown in Fig. 3.4. For 60 Hz, the optimizer does not place any material in the lower box, and the frequency response overlaps the reference curve, indicating that 60 Hz is the resonance frequency of the empty lower box. For the other two designs, the frequency responses show a peak at 30 Hz and 70 Hz, respectively. Here, the lower box acts as a Helmholtz resonator, and the optimizer tunes each frequency under consideration as the resonance frequency of the Helmholtz resonator.

We use octave bands of various widths for multi-frequency optimization. In the octave band, the highest frequency is double that of the lowest. For the numerical experiments, we consider single, one-and-a-half, and double octave bands. The multi-frequency optimization designs along with their frequency responses are presented in Fig. 3.5. All the designs show a distinct bandpass in their respective frequency response. Furthermore, the optimizer adds a wall to all of the designs, effectively resulting in a cascade of two Helmholtz resonators.

3.2 Acoustic Diode, Paper III

3.2.1 Introduction

An acoustic diode, as the name suggests, is a device that only enables acoustic waves to travel in one direction while preventing them from flowing in the opposite direction. Uni-directional acoustic waveguides have application in many biomedical devices such as ultrasonic imaging [35] and lithotripsy [34]. Thus, designing a passive one-way acoustic waveguide is of interest to physicist and engineers. Researchers have used linear [28, 50, 63, 67] as well as non-linear models [14, 23] to design acoustic diodes. The nonlinear models suffer from low transmission efficiency, which motivates efforts to design a linear device. To this end, we employ material distribution based topology optimization to design a uni-directional waveguide based on time harmonic linear wave propagation.

3.2.2 Mathematical Modeling

Consider the axisymmetric setup illustrated in Fig. 3.6, where Ω^{D} is our design domain, and Ω^{W} denotes the left and right waveguides. The left and right waveguides are truncated at Γ^{L} and Γ^{R} by a Dirichlet to Neumann (DTN) type boundary condition. We consider waves traveling towards Ω^{D} as incoming waves and waves traveling away from Ω^{D} as outgoing waves.

The wave propagation inside Ω is governed by the Helmholtz equation for

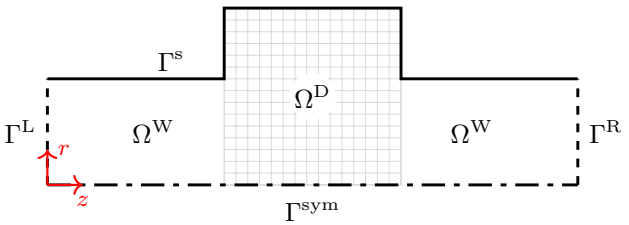

Figure 3.6: Computational domain for two dimensional axi-symmetric setup. Γ^{sym} denotes the axis of symmetry and Γ^{s} denotes the soundhard walls. Γ^{L} and Γ^{R} denote the boundaries of artificially truncated waveguides at left and right, respectively.

the cylindrical coordinates. Thus, the state equation reads:

$$-\nabla \cdot (r\nabla p) - k^2 r p = 0, \qquad \text{in } \Omega, \tag{3.6}$$

$$\frac{\partial p}{\partial n} = 0, \qquad \text{on } \Gamma^{\mathrm{s}} \cup \Gamma^{\mathrm{sym}}, \tag{3.7}$$

$$\frac{\partial p}{\partial n} - \mathrm{DtN}(p) = g^{\mathrm{L}}, \qquad \text{on } \Gamma^{\mathrm{L}}, \tag{3.8}$$

$$\frac{\partial p}{\partial n} - \mathrm{DtN}(p) = g^{\mathrm{R}}, \qquad \text{on } \Gamma^{\mathrm{R}}, \tag{3.9}$$

where g^{L} and g^{R} are the incoming waves in the left and right waveguides, respectively.

3.2.3 Optimization Problem

To design a uni-directional waveguide, we consider the following two cases:

Case 1: An incoming planar wave in the left waveguide traveling towards Ω^{D}.

Case 2: An incoming planar wave in the right waveguide traveling towards Ω^{D}.

The objective of this study is to maximize the power transmission to the right for Case 1 and minimize the power transmission to the left for Case 2. We use scattering parameters, $S_{X_i Y_j}$, to define power (reflection and transmission) in left and right waveguides, where $X \in \{\mathrm{L}, \mathrm{R}\}$, $Y \in \{\mathrm{L}, \mathrm{R}\}$, and $i, j = 0, 1, \ldots, M^{\mathrm{p}}$. Here, the left and right waveguides are denoted by L and R, respectively, and the number of propagating modes is denoted by M^{p}. The definition of $S_{X_i Y_j}$ is

$$S_{X_i Y_j} = \frac{\text{Output power of mode } j \text{ at } \Gamma^Y}{\text{Input power of only mode } i \text{ at } \Gamma^X}. \tag{3.10}$$

Based on definition of scattering parameters, we define the objective function as

$$J\big(\mathcal{F}(\boldsymbol{\alpha})\big) = \sum_{n=1}^{N^{\mathrm{f}}} \sum_{m=0}^{M^{\mathrm{p}}} \Big(S_{\mathrm{L}_0\mathrm{R}_m}(\mathcal{F}(\boldsymbol{\alpha}), \omega_n) + S_{\mathrm{R}_0\mathrm{L}_m}(\mathcal{F}(\boldsymbol{\alpha}), \omega_n) \Big), \tag{3.11}$$

Figure 3.7: Optimized design that only allows uni-directional acoustic flow (left to right) for frequency range 8–9 kHz

where we optimize for a set of angular frequencies $\omega_1, \omega_2, \ldots, \omega_{N^{\mathrm{f}}}$.

3.2.4 Selected Results

For the numerical experiments, we choose the width of left and right waveguides such that they only allow the planar and first non-planar modes to propagate. We optimize this setup for the target frequency range 8–9 kHz. Fig. 3.7 illustrates the optimized design that only allows acoustic waves to travel in one direction (from left to right) for planar incoming waves. Fig. 3.8 presents graphs of transmission and reflection for an incoming planar wave at left and right waveguides. The graph for Case 1 indicates that the optimized design in Fig. 3.7 converts nearly all the power of the planar incoming wave at the left waveguide to the first non-planar wave at the right waveguide. For all frequencies in the range 8–9 kHz, more than 99.8 % of the power is transmitted to the non-planar mode at the right waveguide. Furthermore, for the target frequency band 8-9 kHz, there is approximately no reflection, as $S_{\mathrm{L}_0\mathrm{L}_0} < 5.4 \times 10^{-4}$ and $S_{\mathrm{L}_0\mathrm{L}_1} < 9.0 \times 10^{-4}$, respectively, and nearly no transmission at the planar mode, as $S_{\mathrm{L}_0\mathrm{R}_0} < 2.2 \times 10^{-3}$.

The graph for Case 2 indicates that the optimized design in Fig. 3.7 reflects back nearly all the power of the planar incoming wave at the right waveguide. For all frequencies in the range 8-9 kHz, more than 99.5 % of the power is reflected back to the planar mode at the right waveguide. Furthermore, for the target frequency band 8-9 kHz, there is approximately no transmission, as $S_{\mathrm{R}_0\mathrm{L}_0} < 2.2 \times 10^{-3}$ and $S_{\mathrm{R}_0\mathrm{L}_1} < 4.2 \times 10^{-4}$, respectively, and nearly no reflection at the first non-planar mode, as $S_{\mathrm{R}_0\mathrm{R}_1} < 2.3 \times 10^{-3}$.

The wave propagation in Case 1 and Case 2 is essentially in one direction, from left to right, for the target frequency band. Here, mode conversion is used to generate uni-directional acoustic flow, and our waveguide setup seems to behave as an acoustic diode for an incoming planar wave at the left and right waveguides. Now, we define two more cases to test our optimized design illustrated in Fig. 3.7 with the first non-planar mode as an incoming wave:

Case 3: First non-planar mode as incoming wave in the left waveguide traveling towards Ω^{D}.

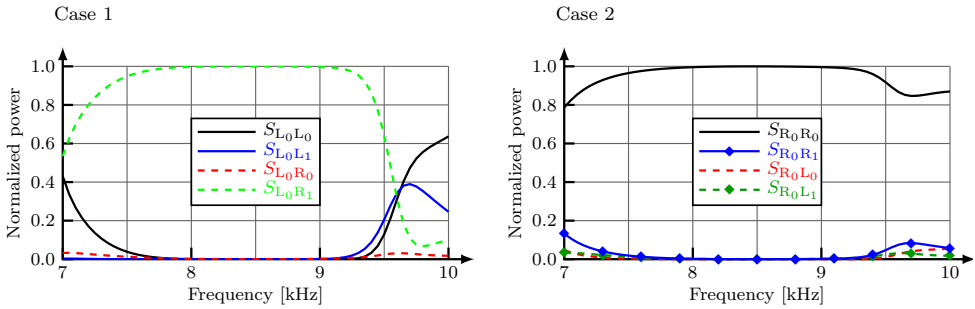

Figure 3.8: Normalized power plotted vs the frequency. Left: Planar incoming wave in the left waveguide. Right: Planar incoming wave in the right waveguide

Case 4: First non-planar mode as incoming wave in the right waveguide traveling towards Ω^{D}.

Fig. 3.9 presents graphs of transmission and reflection for the first non-planar mode as an incoming wave. The graph for Case 3 shows that nearly all the power of incoming first non-planar mode is reflected back. For all frequencies in the range 8-9 kHz, more than 99.7 % is reflected back to the first non-planar mode at left waveguide. Moreover, there is approximately no transmission, as $S_{\mathrm{L_1R_0}} < 4.2 \times 10^{-4}$ and $S_{\mathrm{L_1R_1}} < 9.9 \times 10^{-4}$, respectively, and nearly no reflection at the planar mode, as $S_{\mathrm{L_1L_0}} < 9.0 \times 10^{-4}$, for the target frequency band 8-9 kHz.

The graph for Case 4 shows that nearly all the power of incoming first non-planar mode at left waveguide is converted to the planar mode at right waveguide. For all frequencies in the range 8-9 KHz, more than 99.6 % is transmitted to the first non-planar mode at left waveguide. Moreover, there is approximately no reflection, as $S_{\mathrm{R_1R_0}} < 2.3 \times 10^{-3}$ and $S_{\mathrm{R_1R_1}} < 5.4 \times 10^{-4}$, respectively, and nearly no transmission at the planar mode, as $S_{\mathrm{R_1L_1}} < 9.9 \times 10^{-4}$, for the target frequency band 8-9 kHz.

The results indicate that the optimized design does not act as an acoustic diode for all four cases. Moreover, in order to achieve a uni-directional acoustic flow, the planar mode is converted to the first non-planar mode and vice versa. In fact, all the linear diodes in the literature are mode converters. To design a real acoustic diode, which is a non-linear device, we need to break reciprocity. However, it is possible to design a highly efficient uni-directional waveguide using the linear model when relying on mode conversion.

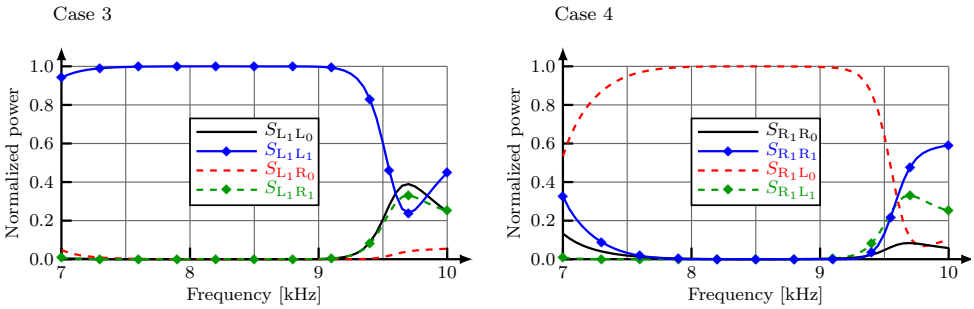

Figure 3.9: Normalized power plotted vs the frequency. Left: First non-planar mode as incoming wave in the left waveguide. Right: First non-planar mode as incoming wave in the right waveguide.

3.3 Frequency Dividing Multiplexer, Paper IV

3.3.1 Introduction

A frequency dividing multiplexer (FDM) is a device that divides the incoming signal into multiple non-overlapping frequency bands and delivers them to their respective output port. This device allows system miniaturization by using a single input port for multiple signals. We employ the material distribution based topology optimization to design an FDM that operates at microwave frequencies. By placing a metallic material within the design domain, the aim is to design a passive device that splits the incoming signal into two frequency bands and transmit them to their respective output ports. The design of metallic FDM using the topology optimization presents two challenging issues. The first issue is that the intermediate values of design variables are associated with Ohmic losses, which makes the optimization problem self penalizing. The second issue is the dependency of optimization results on the formulation of the objective function and the initial design. We solve the self penalizing issue by employing a filtering method and a continuation approach. To solve the second issue, we derive a power balance expression of the device. Using the power balance expression, we formulate three successive objective function, each with an additional parameter. We study the impact of each parameter on the optimization results.

3.3.2 Mathematical Modeling

Consider the three-port setup illustrated in Fig. 3.10. The three waveguides and the design domain Ω^{D} constitute the computational domain Ω. Moreover, Γ_1, Γ_2, and Γ_3 denote the boundaries of three artificially truncated waveguides, and the boundary Γ_{PEC} represent the perfect electric conductor.

We consider the time harmonic Maxwell's equation for the electric field $\boldsymbol{E}$.

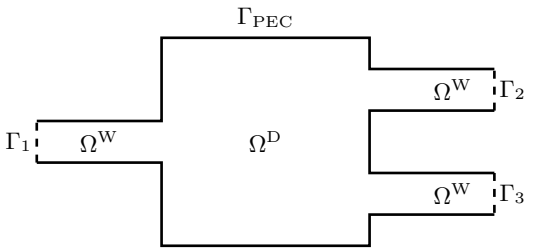

Figure 3.10: Computational domain for three-port frequency dividing multiplexer. The boundary Γ_{PEC} is a perfect electric conductor. Γ_1, Γ_2, Γ_3 indicate port-1, port-2, and port-3, respectively.

Moreover, we assume that the electric field is polarized normal to the plan, that is, $\boldsymbol{E} = (0, 0, u)$, which provides us the Helmholtz equation for u. The metallic boundaries are assumed to be perfect electric conductors and a first-order absorbing boundary condition is used to truncate the domain at Γ_m. Hence, the state equation reads:

$$-\Delta u - k^2\left(\epsilon_r - \mathrm{i}\sqrt{\frac{\mu_0}{\epsilon_0}}\frac{\sigma}{k}\right)u = 0 \qquad \text{in } \Omega, \tag{3.12}$$

$$u = 0 \qquad \text{on } \Gamma_{\mathrm{PEC}}, \tag{3.13}$$

$$\frac{\partial u}{\partial n} + \mathrm{i}Ku = 2\mathrm{i}Kg_mA_m \qquad \text{on } \Gamma_m, \tag{3.14}$$

where the wavenumber $k = \omega/c$, the speed of light $c = \sqrt{1/\mu_0\epsilon_0}$, in which μ_0 and ϵ_0 are the permeability and permittivity in free space, respectively, σ is the electrical conductivity, ϵ_r is the relative permittivity, K is the reduced wavenumber, A_m is the complex amplitudes of incoming waves at port-m, and function g_m is the mode at port-m.

The width of the ports only allow the first non-planar mode to propagate and all higher modes are evanescent. Expression (3.14) for the first-order absorbing boundary condition allows us to set the amplitude of the incoming wave. Furthermore, the governing equation (3.12) along with the Dirichlet condition (3.13) and the first-order absorbing boundary condition (3.14) is discretized using the finite element method.

3.3.3 Optimization Problem

We define P_{mn} to compute the power of transmission, reflection, and cross-coupling in the waveguides. The following expression computes P_{mn} when only port-n is excited

$$P_{mn} = \frac{\text{Output power at port-}m}{\text{Input power at port-}n} \quad m,\, n = 1,\, 2,\, 3. \tag{3.15}$$

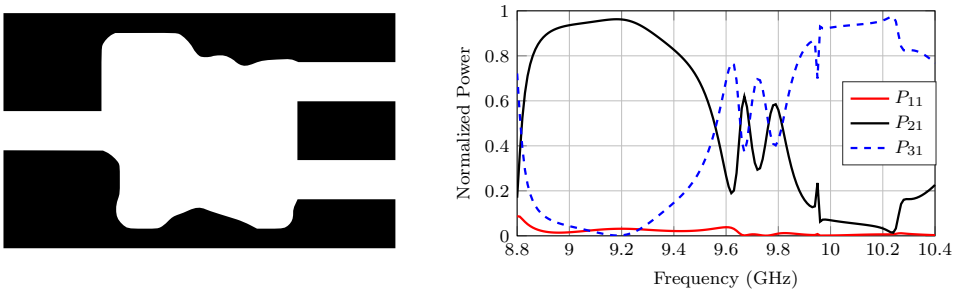

Figure 3.11: Optimized design and its frequency response with the first objective function.

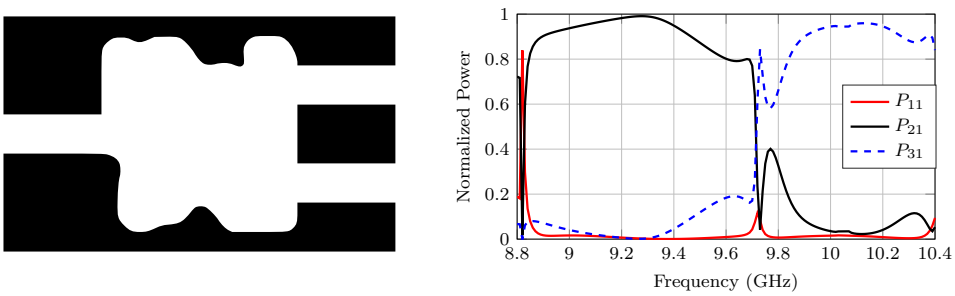

Figure 3.12: Optimized design and its frequency response with the second objective function.

By setting the amplitudes of incoming waves $A_1 = 1$, and $A_2 = A_3 = 0$, the power balance for the device can be written as

$$P_{11} + P_{21} + P_{31} + \text{Ohmic losses} = 1. \tag{3.16}$$

The aim of this study is to maximize P_{21} for frequency band-1 and maximize P_{31} for frequency band-2.

3.3.4 Selected Results

For the numerical experiments, we use 9.0–9.2 GHz as frequency band-1 and 10.0–10.2 GHz as frequency band-2. As stated earlier, we use power balance (3.15) to formulate our objective functions. For the first objective function, we simply consider transmission, that is, P_{21} for frequency band-1 and P_{31} for frequency band-2. The objective function for the transmission is formulated as

$$J_1(\mathcal{F}(\boldsymbol{\alpha})) = \sum_{q=1}^{Q_1} \big(1 - P_{21}(\mathcal{F}(\boldsymbol{\alpha}), k_q)\big) + \sum_{q=Q_1+1}^{Q_1+Q_2} \big(1 - P_{31}(\mathcal{F}(\boldsymbol{\alpha}), k_q)\big), \tag{3.17}$$

where we optimize for the set of wavenumbers $k_1, k_2, \ldots, k_{Q_1+Q_2}$, and Q_1 and Q_2 denote the number of frequencies in frequency band-1 and frequency band-2, respectively. Here, we minimize J_1 to maximize P_{21} for frequency band-1 and P_{31} for frequency band-2. The resulting design, illustrated in Fig. 3.11, shows a good multiplexing effect with $J_1 = 1.1987$ compared to an initial value of $J_1 = 12.2225$ with an empty design domain. We evaluate J_1 to compare all the resulting designs, as it provides a measure of transmission.

We only provide information about transmission to the first objective function. For the second objective function, we add a cross-coupling term to the objective function. More precisely, we add P_{31} for the frequency band-1 and P_{21} for the frequency band-2 to the objective function. To this end, we formulate the following objective function

$$J_2(\mathcal{F}(\boldsymbol{\alpha})) = \sum_{q=1}^{Q_1} \Big(P_{31}(\mathcal{F}(\boldsymbol{\alpha}), k_q) \Big) + \sum_{q=Q_1+1}^{Q_1+Q_2} \Big(P_{21}(\mathcal{F}(\boldsymbol{\alpha}), k_q) \Big). \tag{3.18}$$

Hence, for the second study, we minimize the sum of J_1 and J_2. The final design together with its frequency response is presented in Fig. 3.12. Moreover, the value of $J_1 = 0.9583$, which indicates an improved multiplexing effect compared to the first objective function. For the third objective function, we add information about reflection as well. To do so, we define the following objective function that includes P_{11} for both frequency bands

$$J_3(\mathcal{F}(\boldsymbol{\alpha})) = \sum_{q=1}^{Q_1} \Big(P_{11}(\mathcal{F}(\boldsymbol{\alpha}), k_q) \Big) + \sum_{q=Q_1+1}^{Q_1+Q_2} \Big(P_{11}(\mathcal{F}(\boldsymbol{\alpha}), k_q) \Big). \tag{3.19}$$

Similarly, for the third study, we minimize the sum of J_1, J_2, and J_3. The resulting design and its frequency response are identical to the results of the second objective function. Moreover, the value of $J_1 = 0.9524$ is slightly better than the second objective function, which indicates that adding information on reflection does not improve the results significantly in this case.

The results discussed above were obtained using an empty design domain as an initial design. However, we also performed numerical experiments with different initial designs such as different sizes of triangles, circles, and square shapes. The results indicate that there are multiple good local minima, and we can achieve a good multiplexing effect by selecting a good initial design. Fig. 3.13 illustrate the optimized design with a circle-shaped initial design. In this case, the frequency response for frequency band-1 is flat, and the value of $J_1 = 0.5370$ suggests that the multiplexing effect is much better compared to earlier designs.

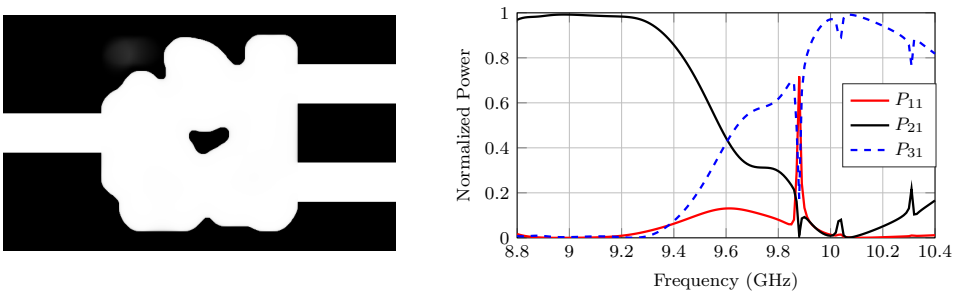

Figure 3.13: Optimized design with and its frequency response with the second objective function and a circle shaped initial design.

3.4 Sensitivity Analysis of a Coupled Plasmonic Problem, Paper V

3.4.1 Introduction

In material distribution-based topology optimization, we define a material indicator function to model the presence and absence of material. Usually, a gradient-based algorithm is used to solve the topology optimization problem. The adjoint method is used to efficiently compute gradients with respect to the design variables. In this study, we perform a sensitivity analysis of a coupled plasmonic problem using the adjoint method. More precisely, a TE-polarized Helmholtz equation is coupled to the Poisson equation. The coupled plasmonic problem poses several challenges due to the complex solution of the TE-polarized Helmholtz equation. Here, we handle these issue by first considering a simple model problem with Poisson-Poisson coupling. By only considering the Poisson problems, we avoid the complex solution of Helmholtz equation. Thus, after examining the model problem, we perform a sensitivity analysis of the coupled plasmonic problem and highlight the main differences.

3.4.2 The Model Problem

Consider the setup, illustrated in Fig. 3.14, for the model problem. The first Poisson problem is

$$\begin{aligned} -\nabla \cdot \eta \nabla u &= 1 \quad \text{in} \quad \Omega, \\ u &= 0 \quad \text{on} \quad \Gamma^{\mathrm{D}}, \\ n \cdot \nabla u &= 0 \quad \text{on} \quad \Gamma^{\mathrm{N}}, \end{aligned} \tag{3.20}$$

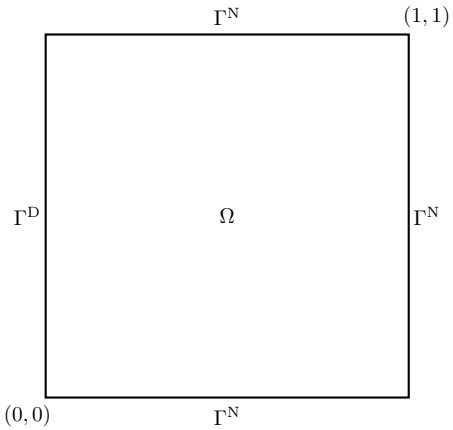

Figure 3.14: Computational domain Ω for the model problem

In the second Poisson problem, η times the square of the solution of first problem (3.20) enters as a forcing term, that is,

$$\begin{aligned} -\nabla \cdot \kappa \nabla T &= \eta\, u^2 \quad \text{in} \quad \Omega, \\ T &= 0 \quad \text{on} \quad \Gamma^{\mathrm{D}}, \\ n \cdot \nabla T &= 0 \quad \text{on} \quad \Gamma^{\mathrm{N}}. \end{aligned} \tag{3.21}$$

A variational form of the first Poisson problem (3.20) is:

$$\begin{aligned} &\text{find } u \in \mathcal{V} \text{ such that} \\ &\int_\Omega \eta \nabla u \cdot \nabla v = \int_\Omega v \quad \forall\, v \in \mathcal{V}, \end{aligned} \tag{3.22}$$

where $\mathcal{V} = \{q \in H^1(\Omega) \big|\, q|_{\Gamma^{\mathrm{D}}} \equiv 0\}$. The variational form of the Poisson problem (3.21) is:

$$\begin{aligned} &\text{find } T \in \mathcal{V} \text{ such that} \\ &\int_\Omega \kappa \nabla T \cdot \nabla q = \int_\Omega \eta\, u^2 q \quad \forall\, q \in \mathcal{V}. \end{aligned} \tag{3.23}$$

In the model problem, the objective function is the integral over Ω.

$$J = \int_\Omega T. \tag{3.24}$$

To perform sensitivity analysis, we first consider design perturbation $\delta\eta$ for the objective function (3.24), and variational forms (3.22) and (3.23), respectively. Given a design perturbation $\delta\eta$, the corresponding first-order perturbation of J is

$$\delta J = \int_\Omega \delta\eta\, u^2\, z^{(1)} - \int_\Omega \delta\eta\, \nabla u \cdot \nabla z^{(2)}, \tag{3.25}$$

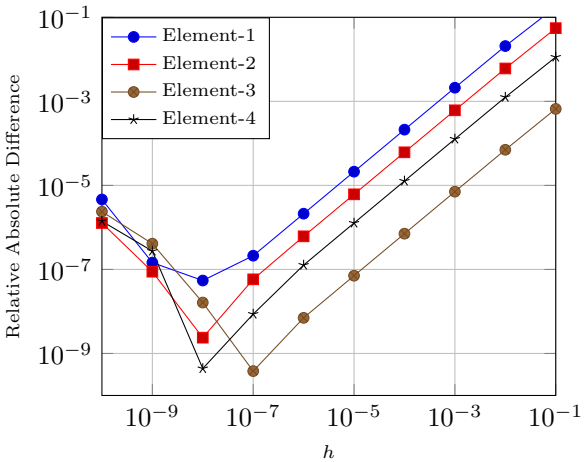

Figure 3.15: The relative absolute difference in gradients of the objective function with respect to η for the model problem, evaluated using the adjoint and the finite difference method, is plotted against the finite difference h for all four elements in the computational domain Ω.

where the two ajoints $z^{(1)}$ and $z^{(2)}$ solve the following two adjoint equations

$$\begin{aligned} &\text{find } z^{(1)} \in \mathcal{V} \text{ such that} \\ &\int_\Omega \kappa \nabla v \cdot \nabla z^{(1)} = \int_\Omega v, \quad \forall\, v \in \mathcal{V}, \end{aligned} \tag{3.26}$$

and

$$\begin{aligned} &\text{find } z^{(2)} \in \mathcal{V} \text{ such that} \\ &\int_\Omega \eta \nabla q \cdot \nabla z^{(2)} = 2 \int_\Omega \eta\, u\, z^{(1)}\, q, \quad \forall\, q \in \mathcal{V}, \end{aligned} \tag{3.27}$$

respectively.

Secondly, we consider design perturbation $\delta\kappa$ and the corresponding first-order perturbation of J is

$$\delta J = -\int_\Omega \delta\kappa \nabla T \cdot \nabla z^{(1)}, \tag{3.28}$$

where the adjoint equation for this problem is similar to Eq. (3.26) for $z^{(1)}$. So, it is sufficient to solve two ajoint equations to obtain sensitivities with respect to η and κ.

For the model problem, we consider a minimal example with just four elements in Ω. We employ the finite difference method to validate our gradients obtained using the adjoint method. The gradients of J with respect to perturbed κ are standard and well known. Therefore, we only validate gradients of J with respect to perturbed η. The absolute relative difference between

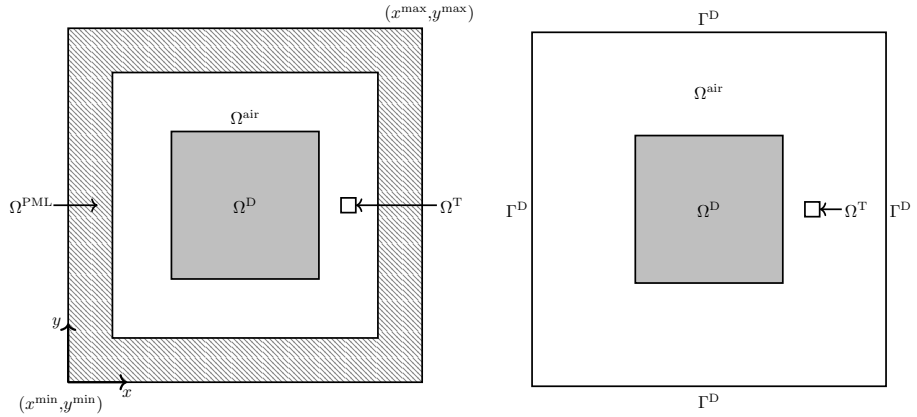

Figure 3.16: Computational domain Ω for the (Left) Plasmonic and (Right) Poisson problem.

the gradients computed using the adjoint and the finite difference approaches converges linearly, as seen in Fig. 3.15.

3.4.3 The Plasmonic Problem

We assume that the wave propagation is governed by the time harmonic Maxwell's equation for magnetic field $\boldsymbol{H}$. In this case, we use $H = (0, 0, u)$ for which the Maxwell equations reduces to the following Helmholtz equation

$$-\nabla \cdot \left(\frac{1}{\epsilon}\nabla u\right) - k^2 u = 0, \tag{3.29}$$

where ϵ is the complex permittivity, $k = \omega/c$ is the wavenumber, ω is the angular frequency, and c is the speed of light. Moreover, the total field u is a combination of incoming and outgoing waves

$$u = u^{\text{in}} + u^{\text{out}}, \tag{3.30}$$

where we assume $u^{\text{in}} = \mathrm{e}^{-\mathrm{i}kx}$.

Substituting u from equation (3.30) in equation (3.29), we obtain

$$\nabla \cdot \left(\frac{1}{\epsilon}\nabla u^{\text{out}}\right) + k^2 u^{\text{out}} = -\left(\frac{1}{\epsilon} - 1\right)\nabla \cdot \nabla u^{\text{in}}. \tag{3.31}$$

In our problem setup, illustrated in Fig. 3.16, parts of Ω^{D} are occupied by silver with a permittivity $\epsilon_{Ag} = -5.0012 + 0.1295\mathrm{i}$ and the rest of $\mathbb{R}^2$ is occupied by air with a permittivity $\epsilon_{air} = 1$. Moreover, the size of Ω^{D} is $100 \times 100\,\text{nm}$ and thickness of Ω^{air} is 60 nm. For the outgoing waves, we add a PML region of

sufficient thickness $d = 40\,\mathrm{nm}$ around Ω^{air}. The variational form of the above equation with PML for outgoing wave u^{out} is:

find $u^{\mathrm{out}} \in H^1(\Omega)$ such that

$$k^2 \int_\Omega \zeta u^{\mathrm{out}} v - \int_\Omega (\boldsymbol{D}\nabla u^{\mathrm{out}}) \cdot \nabla v - \int_{\Omega^{\mathrm{D}}} \eta \nabla u^{\mathrm{out}} = -\int_{\Omega^{\mathrm{D}}} \eta \nabla u^{\mathrm{in}} \cdot \nabla v, \quad v \in H^1(\Omega), \tag{3.32}$$

where $\eta(x) = \frac{1}{\epsilon(x)} - 1$.

We aim to study the temperature in the target region Ω^{T} of size $10 \times 10\,\mathrm{nm}$, with an incoming wave in Ω^{D} at $413\,\mathrm{nm}$. To this end, we couple the Helmholtz equation (3.31) to a Poisson equation of the form

$$\nabla \cdot \kappa \nabla T = \mathrm{Im}(\epsilon) u \bar{u} \quad \text{in} \quad \Omega, \tag{3.33}$$

$$T = T_\infty \qquad \text{on} \quad \Gamma^{\mathrm{D}}, \tag{3.34}$$

where T is the temperature, T_∞ is the ambient temperature, and κ is the thermal diffusivity of the medium. The variational form of Poisson equation (3.33) with boundary condition (3.34) is:

$$\begin{aligned} &\text{Find } T \in \mathcal{V} \text{ such that} \\ &\int_\Omega \kappa \nabla T \cdot \nabla q = \int_\Omega \mathrm{Im}\left(\frac{1}{\eta + 1}\right) u \bar{u}\, q, \quad q \in \mathcal{V}. \end{aligned} \tag{3.35}$$

The objective function to study the temperature integrated over Ω^{T} is

$$J = \int_{\Omega^{\mathrm{T}}} T. \tag{3.36}$$

Similarly, as the model problem, we consider design perturbation $\delta\eta$ for the objective function (3.36)

$$\delta J = \int_{\Omega^{\mathrm{T}}} \delta T, \tag{3.37}$$

variational forms (3.32) and (3.35)

$$k^2 \int_\Omega \zeta \delta u^{\mathrm{out}} v - \int_\Omega (\boldsymbol{D}\nabla \delta u^{\mathrm{out}}) \cdot \nabla v - \int_{\Omega^{\mathrm{D}}} \eta \nabla \delta u^{\mathrm{out}} \cdot \nabla v = \int_{\Omega^{\mathrm{D}}} \delta\eta \nabla u^{\mathrm{out}} \cdot \nabla v - \int_{\Omega^{\mathrm{D}}} \delta\eta \nabla u^{\mathrm{in}} \cdot \nabla v, \quad v \in \mathcal{V}, \tag{3.38}$$

and

$$\int_\Omega \kappa\, \nabla \delta T \cdot \nabla q = \int_{\Omega^{\mathrm{D}}} \delta\, \mathrm{Im}\left(\frac{1}{\eta + 1}\right) u \bar{u}\, q + \int_{\Omega^{\mathrm{D}}} \mathrm{Im}\left(\frac{1}{\eta + 1}\right) \left(\delta u^{\mathrm{out}}\, \bar{u} + u\, \delta \bar{u}^{\mathrm{out}}\right) q \quad \forall\, q \in \mathcal{V}, \tag{3.39}$$

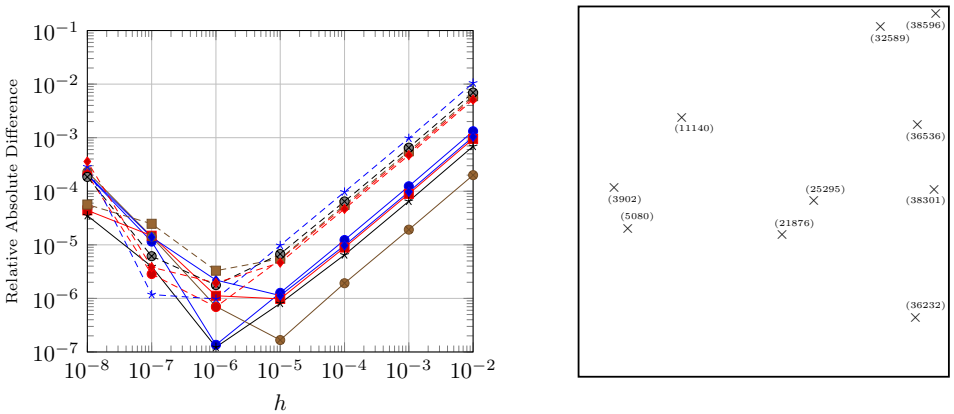

Figure 3.17: Left: The relative absolute difference in gradients of the objective function with respect to η for the plasmonic problem, evaluated using the adjoint and the finite difference method, is plotted against the finite difference h for ten randomly selected elements in the Ω^{D}. Right: Placement of ten randomly selected elements in Ω^{D}.

respectively.

We similarly select the first adjoint $z^{(1)}$ as the problem:

$$\begin{aligned} &\text{find } z^{(1)} \in \mathcal{V} \text{ such that} \\ &\int_{\Omega} \kappa \nabla v \cdot \nabla z^{(1)} = \int_{\Omega^{\mathrm{T}}} v, \quad \forall\, v \in \mathcal{V}. \end{aligned} \tag{3.40}$$

In the following equation, we select $z^{(2)}$ analogous to the model problem in Eq. (3.27):

$$\begin{aligned} &\text{find } z^{(2)} \in \mathcal{V} \text{ such that} \\ &k^2 \int_{\Omega} \zeta\, q\, z^{(2)} - \int_{\Omega} (\boldsymbol{D} \nabla q) \cdot \nabla z^{(2)} - \int_{\Omega^{\mathrm{D}}} \eta \nabla q \cdot \nabla z^{(2)} \\ &\qquad = \int_{\Omega^{\mathrm{D}}} \mathrm{Im}\left(\frac{1}{\eta + 1}\right) \left(q\, \bar{u} + u\, \bar{q}\right) z^{(1)}. \end{aligned} \tag{3.41}$$

Unlike the model problem, there is no $z^{(2)}$ that solves the above equation. In general, to deal with δu^{out} and $\delta \bar{u}^{\mathrm{out}}$ in Eq. (3.39), we need two additional adjoint equations. To handle δu^{out} and $\delta \bar{u}^{\mathrm{out}}$, we select two adjoints $z^{(2)}$ and $z^{(3)}$ in the following two expressions:

find $z^{(2)} \in \mathcal{V}$ such that

$$k^2 \int_\Omega \zeta\, q\, z^{(2)} \; - \int_\Omega (\boldsymbol{D}\nabla q) \cdot \nabla z^{(2)} \; - \int_{\Omega^{\mathrm{D}}} \eta \nabla q \cdot \nabla z^{(2)} \\ = \int_{\Omega^{\mathrm{D}}} \mathrm{Im}\left(\frac{1}{\eta+1}\right) q\, \bar{u}\, z^{(1)}, \quad \forall\, q \in \mathcal{V}. \quad (3.42)$$

and

find $z^{(3)} \in \mathcal{V}$ such that

$$k^2 \int_\Omega \bar{\zeta}\, p\, z^{(3)} \; - \int_\Omega (\overline{\boldsymbol{D}}\nabla p) \cdot \nabla z^{(3)} \; - \int_{\Omega^{\mathrm{D}}} \bar{\eta} \nabla p \cdot \nabla z^{(3)} \\ = \int_{\Omega^{\mathrm{D}}} \mathrm{Im}\left(\frac{1}{\eta+1}\right) p\, u\, z^{(1)}, \quad \forall\, p \in \mathcal{V}, \quad (3.43)$$

respectively. As $z^{(1)}$ is real, thus $z^{(2)} = \bar{z}^{(3)}$, which means that we do not need to compute the third adjoint. Thus, the following expression provides the first order perturbation of objective function (3.36) with respect to perturbed $\delta\eta$,

$$\delta J = \int_{\Omega^{\mathrm{D}}} \delta\, \mathrm{Im}\left(\frac{1}{\eta+1}\right) u\bar{u}\, z^{(1)} + 2 \int_{\Omega^{\mathrm{D}}} \mathrm{Re}\big\{\delta\eta \nabla\big(u^{\mathrm{out}} - u^{\mathrm{in}}\big) \cdot \nabla z^{(2)}\big\}. \quad (3.44)$$

By using the finite element method, we discretize the computational domain into 40,000 elements. For the validation of gradients with the finite difference approach, we randomly select ten elements. Furthermore, as shown in Fig. 3.17, the absolute relative difference between gradients computed using the adjoint and finite difference techniques converges linearly.

Bibliography

[1] Niels Aage and V Egede Johansen. "Topology optimization of microwave waveguide filters". In: *International Journal for Numerical Methods in Engineering* 112.3 (2017), pp. 283–300.

[2] Niels Aage, NA Mortensen, and Ole Sigmund. "Topology optimization of metallic devices for microwave applications". In: *International Journal for numerical methods in engineering* 83.2 (2010), pp. 228–248.

[3] Niels Aage et al. "Giga-voxel computational morphogenesis for structural design". In: *Nature* 550.7674 (2017), pp. 84–86.

[4] Niels Aage et al. "Topology optimization of large scale stokes flow problems". In: *Structural and Multidisciplinary Optimization* 35.2 (2008), pp. 175–180.

[5] Grégoire Allaire and RV Kohn. "Topology optimization and optimal shape design using homogenization". In: *Topology design of structures*. Springer, 1993, pp. 207–218.

[6] Erik Andreassen et al. "Efficient topology optimization in MATLAB using 88 lines of code". In: *Structural and Multidisciplinary Optimization* 43.1 (Nov. 2010), pp. 1–16. DOI: 10.1007/s00158-010-0594-7.

[7] Martin P Bendsøe and Ole Sigmund. "Material interpolation schemes in topology optimization". In: *Archive of applied mechanics* 69.9 (1999), pp. 635–654.

[8] Martin P Bendsøe and Ole Sigmund. *Optimization of structural topology, shape, and material*. Vol. 414. Springer, 1995.

[9] Martin Philip Bendsøe and Noboru Kikuchi. "Generating optimal topologies in structural design using a homogenization method". In: *Computer Methods in Applied Mechanics and Engineering* 71.2 (1988), pp. 197–224. ISSN: 0045-7825. DOI: https://doi.org/10.1016/0045-7825(88)90086-2. URL: https://www.sciencedirect.com/science/article/pii/0045782588900862.

[10] Martin Philip Bendsoe and Ole Sigmund. *Topology optimization: theory, methods, and applications*. Springer Science & Business Media, 2003.

[11] Thomas Borrvall and Joakim Petersson. “Topology optimization of fluids in Stokes flow”. In: *International journal for numerical methods in fluids* 41.1 (2003), pp. 77–107.

[12] Marco Cavazzuti et al. “High performance automotive chassis design: a topology optimization based approach”. In: *Structural and Multidisciplinary Optimization* 44.1 (2011), pp. 45–56.

[13] Shikui Chen and Wei Chen. “A new level-set based approach to shape and topology optimization under geometric uncertainty”. In: *Structural and Multidisciplinary Optimization* 44.1 (2011), pp. 1–18.

[14] Amir Darabi et al. “Broadband passive nonlinear acoustic diode”. In: *Physical Review B* 99.21 (June 2019). DOI: 10.1103/physrevb.99.214305.

[15] Talib Dbouk. “A review about the engineering design of optimal heat transfer systems using topology optimization”. In: *Applied Thermal Engineering* 112 (2017), pp. 841–854.

[16] Ercan M Dede. “Multiphysics topology optimization of heat transfer and fluid flow systems”. In: *proceedings of the COMSOL Users Conference*. 2009.

[17] Cetin B Dilgen et al. “Topology optimization of turbulent flows”. In: *Computer Methods in Applied Mechanics and Engineering* 331 (2018), pp. 363–393.

[18] David C Dobson and Steven J Cox. “Maximizing band gaps in two-dimensional photonic crystals”. In: *SIAM Journal on Applied Mathematics* 59.6 (1999), pp. 2108–2120.

[19] Maria B Dühring, Jakob S Jensen, and Ole Sigmund. “Acoustic design by topology optimization”. In: *Journal of sound and vibration* 317.3-5 (2008), pp. 557–575.

[20] Hans A Eschenauer and Niels Olhoff. “Topology optimization of continuum structures: a review”. In: *Appl. Mech. Rev.* 54.4 (2001), pp. 331–390.

[21] Allan Roulund Gersborg. *Topology optimization of flow problems*. 2007.

[22] Michael B Giles and Niles A Pierce. “An introduction to the adjoint approach to design”. In: *Flow, turbulence and combustion* 65.3 (2000), pp. 393–415.

[23] Itay Grinberg, Alexander F. Vakakis, and Oleg V. Gendelman. “Acoustic diode: Wave non-reciprocity in nonlinearly coupled waveguides”. In: *Wave Motion* 83 (Dec. 2018), pp. 49–66. DOI: 10.1016/j.wavemoti.2018.08.005.

[24] Xu Guo, Weisheng Zhang, and Li Zhang. “Robust structural topology optimization considering boundary uncertainties”. In: *Computer Methods in Applied Mechanics and Engineering* 253 (2013), pp. 356–368.

[25] Emadeldeen Hassan, Eddie Wadbro, and Martin Berggren. "Topology optimization of metallic antennas". In: *IEEE Transactions on Antennas and Propagation* 62.5 (2014), pp. 2488–2500.

[26] Behrooz Hassani and Ernest Hinton. "A review of homogenization and topology optimization I—homogenization theory for media with periodic structure". In: *Computers & Structures* 69.6 (1998), pp. 707–717.

[27] Behrooz Hassani and Ernest Hinton. *Homogenization and structural topology optimization: theory, practice and software*. Springer Science & Business Media, 2012.

[28] Zhaojian He et al. "Asymmetric acoustic gratings". In: *Applied Physics Letters* 98.8 (2011), p. 083505.

[29] Kristian Ejlebjærg Jensen. *Performing Topology Optimization with the Density Method*. 2019. URL: https://www.comsol.com/blogs/performing-topology-optimization-with-the-density-method/.

[30] Fotios Kasolis, Eddie Wadbro, and Martin Berggren. "Analysis of fictitious domain approximations of hard scatterers". In: *SIAM Journal on Numerical Analysis* 53.5 (2015), pp. 2347–2362.

[31] Hans Petter Langtangen and Svein Linge. *Finite difference computing with PDEs: a modern software approach*. Springer Nature, 2017.

[32] Mats G Larson and Fredrik Bengzon. *The finite element method: theory, implementation, and applications*. Vol. 10. Springer Science & Business Media, 2013.

[33] Jin Woo Lee and Yoon Young Kim. "Topology optimization of muffler internal partitions for improving acoustical attenuation performance". In: *International journal for numerical methods in engineering* 80.4 (2009), pp. 455–477.

[34] Bin Liang, Bo Yuan, and Jian-chun Cheng. "Acoustic diode: Rectification of acoustic energy flux in one-dimensional systems". In: *Physical review letters* 103.10 (2009), p. 104301.

[35] Bin Liang et al. "Frequency-dependence of the acoustic rectifying efficiency of an acoustic diode model". In: *Applied Physics Letters* 96.23 (2010), p. 233511.

[36] Kai Liu and Andrés Tovar. "An efficient 3D topology optimization code written in Matlab". In: *Structural and Multidisciplinary Optimization* 50.6 (June 2014), pp. 1175–1196. DOI: 10.1007/s00158-014-1107-x.

[37] Shutian Liu and Heting Qiao. "Topology optimization of continuum structures with different tensile and compressive properties in bridge layout design". In: *Structural and Multidisciplinary Optimization* 43.3 (2011), pp. 369–380.

[38] AG Michell. "The limits economy in frame structures". In: *Philo. Mag. Sect* 6.8 (1904).

[39] HP Mlejnek. “Some aspects of the genesis of structures”. In: *Structural optimization* 5.1 (1992), pp. 64–69.

[40] Fadl Moukalled, L Mangani, Marwan Darwish, et al. *The finite volume method in computational fluid dynamics*. Vol. 113. Springer, 2016.

[41] Tsuyoshi Nomura et al. “Structural topology optimization for the design of broadband dielectric resonator antennas using the finite difference time domain technique”. In: *International Journal for Numerical Methods in Engineering* 71.11 (2007), pp. 1261–1296.

[42] Daniel Noreland. “Impedance boundary conditions for acoustic waves in a duct with a step discontinuity”. In: *Computer methods in applied mechanics and engineering* 71.2 (2003), pp. 197–224.

[43] Renato Picelli, Raghavendra Sivapuram, and Yi Min Xie. “A 101-line MATLAB code for topology optimization using binary variables and integer programming”. In: *Structural and Multidisciplinary Optimization* 63.2 (2021), pp. 935–954.

[44] W. Prager and G.I.N. Rozvany. “Optimization of structural geometry”. In: *Dynamical Systems*. Ed. by A.R. Bednarek and L. Cesari. Academic Press, 1977, pp. 265–293. ISBN: 978-0-12-083750-2. DOI: https://doi.org/10.1016/B978-0-12-083750-2.50023-0.

[45] George IN Rozvany. “A critical review of established methods of structural topology optimization”. In: *Structural and multidisciplinary optimization* 37.3 (2009), pp. 217–237.

[46] George IN Rozvany. “Aims, scope, methods, history and unified terminology of computer-aided topology optimization in structural mechanics”. In: *Structural and Multidisciplinary optimization* 21.2 (2001), pp. 90–108.

[47] O. Sigmund. “A 99 line topology optimization code written in Matlab”. In: *Structural and Multidisciplinary Optimization* 21.2 (Apr. 2001), pp. 120–127. DOI: 10.1007/s001580050176.

[48] Ole Sigmund and Kurt Maute. “Topology optimization approaches”. In: *Structural and Multidisciplinary Optimization* 48.6 (2013), pp. 1031–1055.

[49] Stoyan Slavov and Mariya Konsulova-Bakalova. “Optimizing Weight of Housing Elements of Two-stage Reducer by Using the Topology Management Optimization Capabilities Integrated in Solidworks: A Case Study”. In: *Machines* 7.1 (2019). ISSN: 2075-1702. DOI: 10.3390/machines7010009.

[50] Ai-Ling Song et al. “Waveform-preserved unidirectional acoustic transmission based on impedance-matched acoustic metasurface and phononic crystal”. In: *Journal of Applied Physics* 120.8 (2016), p. 085106.

[51] Mathias Stolpe and Martin P Bendsøe. “Global optima for the Zhou–Rozvany problem”. In: *Structural and Multidisciplinary Optimization* 43.2 (2011), pp. 151–164.

[52] Katsuyuki Suzuki and Noboru Kikuchi. “A homogenization method for shape and topology optimization”. In: *Computer methods in applied mechanics and engineering* 93.3 (1991), pp. 291–318.

[53] Krister Svanberg. “The method of moving asymptotes—a new method for structural optimization”. In: *International journal for numerical methods in engineering* 24.2 (1987), pp. 359–373.

[54] Krister Svanberg and Henrik Svärd. “Density filters for topology optimization based on the Pythagorean means”. In: *Structural and Multidisciplinary Optimization* 48.5 (2013), pp. 859–875.

[55] Krister Svanberg and Mats Werme. “Topology optimization by a neighbourhood search method based on efficient sensitivity calculations”. In: *International journal for numerical methods in engineering* 67.12 (2006), pp. 1670–1699.

[56] Matthew Tomlin and Jonathan Meyer. “Topology optimization of an additive layer manufactured (ALM) aerospace part”. In: *Proceeding of the 7th Altair CAE technology conference*. 2011, pp. 1–9.

[57] Semyon V Tsynkov. “Numerical solution of problems on unbounded domains. A review”. In: *Applied Numerical Mathematics* 27.4 (1998), pp. 465–532.

[58] Eddie Wadbro and Martin Berggren. “Topology optimization of an acoustic horn”. In: *Computer methods in applied mechanics and engineering* 196.1-3 (2006), pp. 420–436.

[59] Eddie Wadbro and Linus Hägg. “On quasi-arithmetic mean based filters and their fast evaluation for large-scale topology optimization”. In: *Structural and Multidisciplinary Optimization* 52.5 (2015), pp. 879–888.

[60] Eddie Wadbro, Rajitha Udawalpola, and Martin Berggren. “Shape and topology optimization of an acoustic horn–lens combination”. In: *Journal of Computational and Applied Mathematics* 234.6 (2010), pp. 1781–1787.

[61] Jian Wang et al. “Antenna radiation characteristics optimization by a hybrid topological method”. In: *IEEE Transactions on Antennas and Propagation* 65.6 (2017), pp. 2843–2854.

[62] Michael Yu Wang, Xiaoming Wang, and Dongming Guo. “A level set method for structural topology optimization”. In: *Computer methods in applied mechanics and engineering* 192.1-2 (2003), pp. 227–246.

[63] Xiao-Peng Wang et al. “Broadband acoustic diode by using two structured impedance-matched acoustic metasurfaces”. In: *Applied Physics Letters* 109.4 (2016), p. 044102.

[64] Ali Riza Yildiz. “Optimal structural design of vehicle components using topology design and optimization”. In: *Materials Testing* 50.4 (2008), pp. 224–228.

[65] M Zhou and GIN Rozvany. “The COC algorithm, Part II: Topological, geometrical and generalized shape optimization”. In: *Computer methods in applied mechanics and engineering* 89.1-3 (1991), pp. 309–336.

[66] Mingdong Zhou et al. “Industrial application of topology optimization for combined conductive and convective heat transfer problems”. In: *Structural and Multidisciplinary Optimization* 54.4 (2016), pp. 1045–1060.

[67] Yi-Fan Zhu et al. “Acoustic one-way open tunnel by using metasurface”. In: *Applied Physics Letters* 107.11 (2015), p. 113501.

[68] Ji-Hong Zhu, Wei-Hong Zhang, and Liang Xia. “Topology optimization in aircraft and aerospace structures design”. In: *Archives of Computational Methods in Engineering* 23.4 (2016), pp. 595–622.

[69] Zhi Hao Zuo and Yi Min Xie. “A simple and compact Python code for complex 3D topology optimization”. In: *Advances in Engineering Software* 85 (July 2015), pp. 1–11. DOI: 10.1016/j.advengsoft.2015.02.006.